## Introduction

Studies focusing on landslides occurring directly in moraine deposits or moraine ridges are scarce (Beló et al. 2006), even though they have potential to trigger impact waves responsible for the generation of glacial lake outburst floods (Fig. 1). Glacial lake outburst floods have been responsible for large economic costs and the loss of thousands of lives worldwide (Iribarren Anacona et al. 2014). In Cordillera Blanca, Peru (Zapata 2002), different types of slope movements (e.g., landslides, and rockslides) caused 35 % of documented glacial lake outburst floods with known cause (Emmer and Cochachin 2013). These slope movements in previously glaciated regions have often been related to the effects of multiple glacier retreats that result in the debuttressing of bedrock, as well as in debris-mantled slopes and the deposition of steeply inclined glacier sediments (Holm et al. 2004; Hugenholtz et al. 2008). It has been documented that the removal of ice-buttress support has affected landslide occurrence on several lateral moraines worldwide. One example is a compound landslide on the southeast lateral moraine of Palcacocha Lake, which caused a minor glacial lake outburst flood in 2003 (Cordillera Blanca, Peru, Vilímek et al. 2005). Debuttressing also contributed to the activity of large landslides on the moraine of Athabasca glacier in the Canadian Rocky Mts. (Hugenholtz et al. 2008) and resulted in moraine landslides with volumes of up to $0.7 \times 10^6$ m$^3$ in the Alps (i.e., Lower Grindelwald Glacier, Oppikofer et al. 2008; Huggel et al. 2013).

The mechanical and hydrological properties of the moraine slopes are the key to their stability and the possible characteristics of landslides occurring in their material. Only a limited number of studies have dealt with this topic, partly due to methodological constraints in investigating materials with a heterogeneous mix of particles varying from silt to boulders. The significant effects of the fine fraction of the moraine material on its overall strength have been described by Novotný and Klimeš (2014), who argued that suction occurring within this material affects the peak shear strength of the unsaturated moraine material (Simeoni et al. 2003; Springman et al. 2003). Other studies underline the importance of mineral composition, attributing lower strength to sand and gravel soils containing greater proportions of quartz, while increased feldspar composition leads to higher strength due to the greater angularity of the particles (Bolton 1986; Bareither et al. 2008). Slope stability calculations for this environment are even scarcer (Hubbard et al. 2005) and very often involve moraine material situated in contrasting geological settings, e.g., forming the sliding plane of a rock slide (Schneider-Muntau and Zangerl 2005) or moraine deposits overlaying marls (Simeoni et al. 2003).

Another way to better assess potential future landslide hazard is to investigate rates of past movements (Viero et al. 2010; Strozzi et al. 2013; Sun et al. 2015), which ideally cover prolonged time periods and include monitoring of explanatory variables (e.g., ground water levels, pore pressures). In remote high mountain regions where none of these data are available, remote sensing is a suitable alternative for detecting past movements of different landforms (e.g., rock glaciers—Emmer et al. 2015), including landslides (Farina et al. 2006; Righini et al. 2011; Tamburini et al. 2011; Cigna et al. 2012; Hölbling et al. 2012; Strozzi et al. 2013). Spaceborne Synthetic Aperture Radar (SAR) data and related interferometry techniques allow the detection of movement over wide areas with millimeter precision, usually representing total displacements over periods of years.

The initiation and propagation of glacial lake outburst floods are a complex phenomenon that has rarely been studied considering all the different processes involved (Westoby et al. 2014). The complex chain modeling of documented, but unmeasured glacial lake outburst floods is presented, for example, in Worni et al.

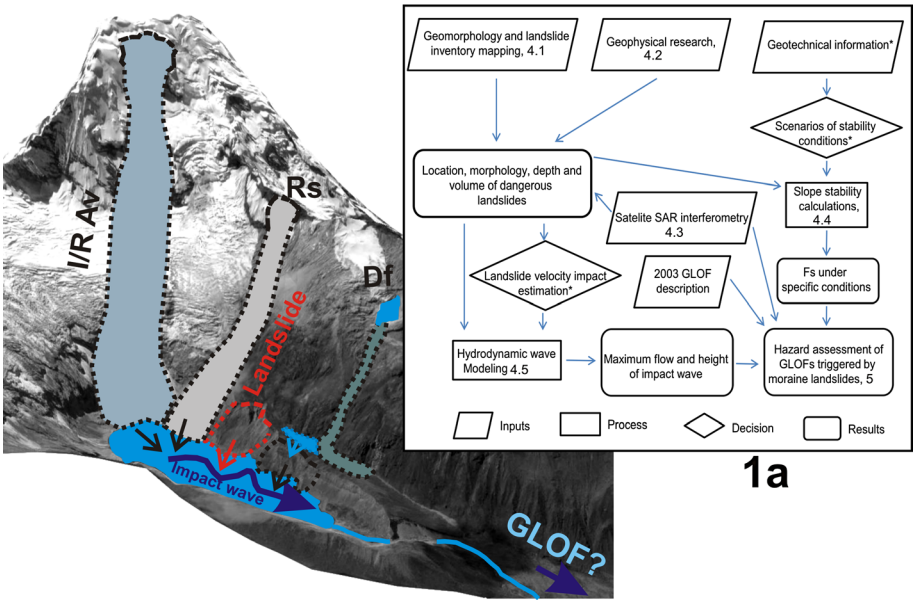


**Fig. 1** Schematic diagram showing theoretical types of slope processes which could triggered GLOFs in the Cordillera Blanca Mts., Peru, representing only fraction of all possible GLOF initiation processes (Emmer and Cochachin 2013; Richardson and Reynolds 2000). Ice/rock avalanche (*I/R Av*) caused the 2010 GLOF from Lake 513 (Klimeš et al. 2014; Schneider et al. 2014); rockslide (*Rs*) initiated the 2002 GLOF from Safuna Alta Lake (Hubbard et al. 2005); landslide from lateral moraine caused the 1953 GLOF from Tullparaju Lake (Lliboutry et al. 1977a), the 2003 GLOF from Palcacocha Lake (Vilímek et al. 2005), and the 2012 GLOF from Artizon Alto Lake (Emmer et al. 2014); a debris flow (*Df*) from a valley dammed temporal lake, which initiated a landslide from the inner slope of the Cangrajanca Lake lateral moraine (Cordillera Huayhuash, Peru, Engel et al. 2011). **a** Workflow diagram showing the steps taken to achieve complex knowledge of processes and conditions affecting hazard imposed by GLOFs triggered by landslides originating in the lateral moraines of the Palcacocha Lake. *Asterisks* indicate steps where review of available literature was extensively used. *Ch.* chapter, *Fs* factor of safety

(2014) or Schneider et al. (2014). The latter is an example from the Cordillera Blanca using Rapid Mas Movement Simulation (RAMMS) for modeling a triggering ice avalanche; wave generation and propagation are modeled using the Iber hydrodynamic model, which provides outflow hydrographs that in turn are used for glacial lake outburst flood modeling, also using RAMMS.

This study aims at an evaluation of landslides from moraine slopes as potential triggers of glacial lake outburst floods. We carried out a variety of research activities, including detailed field data collection, satellite SAR interferometry (InSAR), stability calculations, and hydrodynamic modeling at Palcacocha Lake, Cordillera Blanca, Peru.

## Study area

Palcacocha Lake is situated in the upper part of the Cojup glacial valley (4562 m above sea level (a.s.l.), Fig. 2), which is carved into granites and granodiorites of the Cordillera Blanca batholith (Morales 1967, Estudios glaciologicos-geologicos efectuados en la Cordillera Blanca (in Spanish), unpublished report). This lake produced a catastrophic glacial lake outburst flood in 1941 (Oppenheim 1946; Zapata 2002) and another minor outburst flood in 2003 (Vilímek et al. 2005). The lake's dramatic increase in volume (Somos-Valenzuela et al. 2014), unstable moraines, and the increasing vulnerability of the growing city of Huaráz located downstream made it a suitable site for study.

The inclination of the trough slopes varies between 60° and 80°close to the ridges, dropping to 30°–40° near the valley floor, where the slopes are often covered by talus (Vilímek et al. 2005). The Cordillera Blanca foothills and the Santa River Valley are underlain by sedimentary and volcanic rocks of Mesozoic age. In this area, the Cojup River flows mainly through glaciofluvial deposits, where it has carved a deeply incised canyon-like valley with numerous bank scours. The valley floor progressively flattens and finally opens into an alluvial cone, where the city of Huaráz is located and the Cojup River joints the Quilcay River, which in turn flows into the Santa River at an elevation of 3000 m a.s.l.

Palcacocha Lake is one of almost 600 lakes in the Cordillera Blanca mountain range dammed by moraines (Vilímek et al. 2015). Its current moraine developed during the Little Ice Age, in which the first phase culminated in the Cordillera Blanca between 1590 and 1720 AD (Rabatel et al. 2013). Its terminal moraine (Fig. 2) rises up to146 m above the valley floor. It was filled by lake water until 13 December 1941, when it breached, producing a catastrophic outburst flood that claimed thousands lives in the regional capital city of Huaráz (Lliboutry et al. 1977a; Zapata 2002; Carey 2010). The triggering factor is unknown, but no earthquake was reported before the outburst. Thus, ice fall or glacier calving seems to be possible explanations (Oppenheim 1946). Oppenheim (1946) pointed out that another possibility is dam failure without any external trigger (see also Costa and Schuster 1988), due to (i) internal erosion (widening) of subsurface channels leading to the degradation of dam body and to its rupture (e.g., Richardson and Reynolds 2000) or (ii) spontaneous incision of a surficial outlet in the dam, followed by increasing discharge and additional erosion and incision, and thus progressive enlargement of the dam breach (positive feedback; Yamada 1998). Since then, the stability of the lake dam and possible processes for glacial lake outburst flood initiation have been an important topic for Peruvian and international scientists, as well as for the local community (Carey 2005).

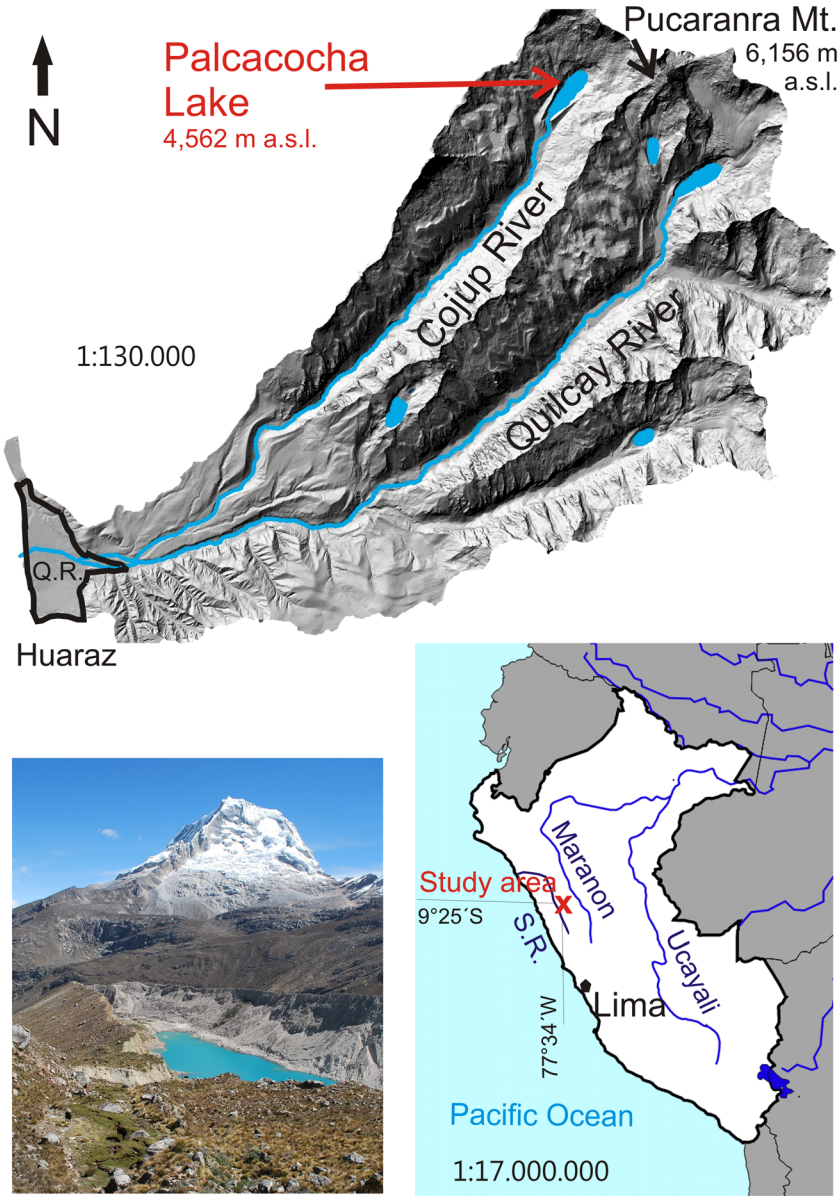


**Fig. 2** Palcacocha Lake and its surrounding on the 5-m DEM (Horizons South America S.A.C., 2013, Informe Técnico del Proyecto, Consultoría Para El Levantamiento Fotogramétrico Detallado De La Sub Cuenca Del Río Quillcay Y La Ciudad De Huaráz BID-MINAM (PE-T 1168)) and on a photograph looking NW, toward Ranrapalca Mt. (6162 m a.s.l.) showing east-facing inner slopes of its terminal moraine; *S.R.* Santa River, *Q.R.* Quilcay River

After the 1941 event, the lake was dammed by a wide moraine with low relief resting on the bottom of the previous lake. It is among about 40 lake dams in the Cordillera Blanca where remedial works were carried out (Reynolds 2003; Portocarrero 2014; Emmer et al. 2016). The dam was reinforced in the early 1970s by two concrete dams with an outflow channel that keeps the water elevation constant at 4562 m a.s.l. (Ojeda 1974). Since 1970, the glacier tongue has retreated by more than 1200 m and the lake volume has increased to a recent volume of about 17 million $m^3$ (Instituto Nacional de Defensa Civil 2011).

A glacial lake outburst flood triggered by a landslide into the lake occurred on March 19, 2003. The landslide was probably caused by saturation of the moraine material by heavy rain. It created a wave more than 8 m high that overtopped the lake dam and resulted in a minor flood in the Cojup Valley, blocking a main Huaráz drinking water treatment facility with sediments. As result of this event, the inhabitants of the Huaráz were without a drinking water supply for more than a week (URGH (2003): Informe técnico: Estado situacional de la laguna Palcacocha (in Spanish). ANA, p 19). Earlier works suggested that the retreat of the glacier tongue, which intensified after 1980, contributed to the landslide initiation (Emmer et al. 2014; Vilímek et al. 2005). Investigations of mechanical and strength properties showed that the inner moraine walls maintain stability despite their very steep slopes (very often above 50°), which exceed the slope angle of tested strength parameters (e.g., angle of repose), which reach values of around 40° (Novotný and Klimeš 2014). This can be partly explained by additional factors affecting the slope stability, including secondary cementation of the sediment, wedged boulders, or the sedimentary structure of the moraine, with additional strength imparted by

large rock slabs oriented perpendicular to the direction of possible shear planes, and interlocking soil strength has to be applied.

## Methods

Field research, satellite SAR interferometry, and numerical analysis were carried out (Fig. 1a) to define realistic conditions needed for assessment of glacial lake outburst floods triggered by landslides from the lateral moraines. Field geomorphological mapping was supported by analyses and interpretation of satellite images (SPOT image from 5.8.2006, Google Earth image from 20.8.2013) and historical aerial photographs (15.7.1950, SAN Perú; August 1970, NASA) to prepare a geomorphological and landslide inventory map of the Palcacocha Lake terminal and lateral moraines. The geomorphological map defined landforms based on their morphology and formative processes. It focused on identifying landslides and describing their current activity during the field research. Fresh-looking features with opened cracks were classified as active, while those more obscured by vegetation and denudation were considered as inactive. The map also shows basic hydrological information, focusing on describing possible sources of seepage water (e.g., streams, springs) in the moraine slopes, during the dry season (May–September) when fieldwork was conducted.

In contrast to geomorphological mapping that defines landslides according to visible morphological features and the presence of sliding planes, differential SAR interferometry (DInSAR; Bamler and Hartl 1998; Rosen et al. 2000) and Persistent Scatterer Interferometry (PSI; Wegmüller et al. 2003; Werner et al. 2003) were used to determine the state of activity of landslides based on displacement rates derived from the interferometric signals (Farina et al. 2006; Righini et al. 2011; Cigna et al. 2012; Hölbling et al. 2012; Strozzi et al. 2013). In this study, DInSAR and PSI have been applied to stacks of high-resolution ERS-1/2 SAR, ENVISAT ASAR, and ALOS PALSAR (ground resolution on the order of 20 m) and very-high-resolution TerraSAR-X images (ground resolution on the order of 3 m) acquired between 1992 and 2015 (Table 1). Images from ascending and descending orbits were analyzed for better spatial coverage around the lake. Snow cover did not cause phase decorrelation in the interferograms, and therefore, all scenes could be included in the analysis. PSI analysis was conducted using only the stacks of ENVISAT ASAR images of the descending orbit and of ALOS PALSAR images of the ascending orbit, because for the other image stacks, the number of acquisitions was insufficient for this kind of processing. PSI results consist of linear deformation rates and displacement histories in the satellite line-of-sight (LOS) direction. Reference points were selected individually for each of the sensors in areas estimated as stable. The error of the average ENVISAT ASAR displacement rates ranges from 1.0 to 1.8 mm year$^{-1}$ (Crosetto et al. 2009) that of the ALOS PALSAR displacement rates is better than 9 mm year$^{-1}$ (Ng et al. 2012). In DInSAR analysis, displacement is derived from the interpretation of the phase difference of the signals acquired by two satellite SAR acquisitions after compensation for topographic effects using an external digital elevation model (DEM) with 5 × 5-m pixel size derived from LiDAR measurements (unpublished report of Horizons South America S.A.C., 2013 Informe Técnico del Proyecto, Consultoría Para El Levantamiento Fotogramétrico Detallado De La Sub Cuenca Del Río Quillcay Y La Ciudad De Huaráz BID-MINAM (PE-T 1168), Ministerio Del Ambiente A Travel Del Fonam, Lima, Peru). Zones with similar displacement rates were identified by interpretation of wrapped interferometric phase images, following recommendations given in Barboux et al. (2014) for interpreting DInSAR signals in mountainous areas. Final determination of whether such zones represent landslides was based on field inventory mapping. As a rule of thumb, an error estimate of one fourth of a phase cycle is considered for the DInSAR images to be a consequence of atmospheric artifacts (Strozzi et al. 2001).

Electric resistivity tomography (ERT) profiles were measured using a 4point light hp earth resistivity meter (Fischer et al. 2013) with electrode spacing of 4 or 2 m, applying Schlumberger, Wenner, and dipole-dipole array settings. The system allowed a maximum profile length of 96 m; therefore, it was necessary to roll up sections to extend the profiles. Due to the sloping unstable sediment, it was not possible to ground the electrodes on the steep inner slopes of the moraine, so the profiles end at the crest of the moraine rim. The maximum acquired length and depth reach by the profiles were 120 and 12.5 m, respectively. The data were processed in the specialized software Res2DInv (by Geotomo Software, Inc.), and the inversion procedure included the effect of the topography of the profiles. The topographic profiles were measured using a hand-held laser inclinometer (LaserAce 1000) with a precision of 0.05 m per 150 m, which allowed all important morphological features to be captured.

Slope stability calculations were carried out for a topographic profile (Fig. 3) across a potentially active compound landslide in the position of profile no. 1 (ERT1 on Fig. 7). Smaller, secondary landslides of the compound, potentially active landslide were considered for the calculations. The calculations were done in GeoSlope software, applying a limit equilibrium method (Morgenstern and Price 1965). The potential sliding surface (e.g., fully specified slip surface) was determined using field mapping and the results of resistivity tomography sounding, which clearly showed its depth, shape, and down-slope limit on the inner moraine slope. Shear strengths of the moraine material were derived from standard and large shear box tests and laboratory tests of angle of repose published in Novotný and Klimeš (2014). The tested soil sample was taken from the landslide scarp. These tests allowed application of peak strength and strength in a critical state to the stability calculations (Fig. 3). Laboratory tests determining minimum and maximum compaction of the material were used to estimate a value of the bulk density of the in situ material, with the value being close to the maximum compaction. It was estimated to be $\gamma = 20$ kN/m$^3$. The moraine material was divided into homogenous layers parallel with the surface of the profile, which were characterized by specific stresses and respective peak shear strengths determined using large shear box tests (Fig. 3b). The stability calculations reflected variability in water content within the moraine material (applied as pore pressure coefficient $r_u$ in the calculations, where $r_u$ represents the portion of water above slip surface) and the effects of earthquakes, introduced as a value of seismic $k_h$ coefficient, which is the ratio of horizontal acceleration to the gravitational acceleration constant. The role of ice support at the slope toe was also tested, but the possible effects of water-level fluctuations were not considered, as the outflow from the lake is fixed by a control structure.

For the hydrodynamic wave modeling, we used the LiDAR-derived 5 × 5-m DEM and bathymetric data measured in the field

**Table 1** Satellite SAR data considered in our study (A: ascending orbit, D: descending orbit)

| Sensor | Track | Time period | No. of images | Time interval (days) |
|---|---|---|---|---|
| ERS-1/2 SAR | D 440 | 2003–2010 | 12 | 35 |
| *ENVISAT ASAR* | *D 440* | *2003–2010* | *21* | *35* |
| ERS-1/2 SAR | A 218 | 1996–1999 | 7 | 35 |
| ENVISAT ASAR | A 261 | 2006–2009 | 13 | 35 |
| *ALOS PALSAR* | *A 111* | *2007–2011* | *19* | *46* |
| TerraSAR-X | D 066 | 2014–2015 | 2 | 11 |

PSI was conducted with stacks of ENVISAT ASAR images of the descending orbit and ALOS PALSAR images of the ascending orbit (italic)

in October 2003, using Humminbird 100SX sonar (unpublished report of URGH, 2003 Informe técnico: levantamiento batimetrico y topográfico de la laguna Palcacocha (in Spanish), ANA). The Iber hydrodynamic model (Iber 2010) allows simulations of turbulent free-surface unsteady flow (Schneider et al. 2014) using input information about the volume of the falling mass and its velocity, with the volume as the critical parameter for the wave type and energy (Panizzo et al. 2005). The landslide volumes were estimated using results of detailed geomorphological mapping (defining aerial extend of the landslides) including topographic profiles, ERT measurements (providing information about possible depths of the main sliding planes of the landslides), and evaluation of pre-failure aerial photographs (1970). The measured aerial extents of the landslide bodies were multiplied by estimated depths of the main sliding planes to provide an estimate of the landslide volume. The modeling approach used information about the 2003 landslide (aerial extent, depth of the sliding plane) and triggered impact wave height to calibrate the model parameters (e.g., impact wave velocity), which were then used to model the possible impact waves caused by the potentially active landslides identified on the moraine. The model results provide maximum wave height and flow volumes. The wave height was compared with a description of the 2003 historical glacial lake outburst flood initiated by a landslide into the lake (Vilímek et al. 2005). Comparison of the historical event with modeled scenarios was used to assess possible future glacial lake outburst flood magnitudes and the degree of hazard caused by the specified outburst flood initiation process.

## Results

### Geomorphological and landslide mapping of the Palcacocha Lake moraine

The general morphology of the lateral moraines and the lake basin is shown on two topographic profiles (b on Fig. 4), which illustrate the gentler inclination of the outer slopes (around 35°) compared to the inner moraine slopes (over 50°), where the majority of the debris flows and landslides occur. No active landforms were identified on the outer slopes. This general observation holds also for available historical information. The outer slopes show some elongated and concave landforms. Some of them were identified on the July 1950 and August 1970 aerial photographs, and some of them were also identified on a photograph by Hanz Kinzl (1932). This

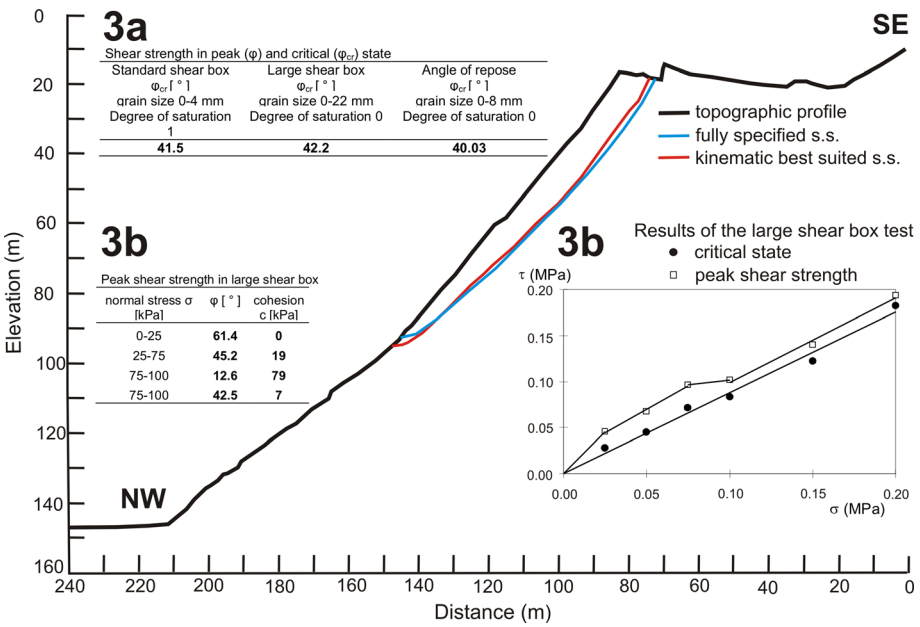


**Fig. 3** Shear strength in peak ($\phi$) and critical ($\phi_{cr}$) state and topographic profile used for slope stability calculation in GeoSlope software (*s.s.* slip surface)

suggests that at least some are more than 80 years old and originated as debris flows or lake spillways formed during the lake development (1 on Fig. 4). However, they could be even older and could have formed during the initial moraine development, when the glacier completely filled the space behind the moraines (2 on Fig. 4). The historical aerial photographs confirm landslide activity on the inner slopes. A shallow landslide on the northwest lateral moraine failed after August 1970, and more recently, a smaller landslide (3 on Fig. 4) was detected in roughly the same spot. The southeast lateral moraine shows a clearly visible scarp, parallel to its crest, in the 1950 image, which 20 years later developed into a landslide about 400 m wide. Part of this landslide remained until recent times (4 on Fig. 4), whereas the rest failed and was replaced by several recently documented landslides described in detail later (5 and 6 on Fig. 4).

The inner slope of the southeast lateral moraine is dominated by a compound landslide formed by a temporarily inactive landslide from March 2003 (6 on Fig. 4) and an active debris flow (6a on Fig. 4). The 2003 landslide triggered an impact wave, which resulted in a minor glacial lake outburst flood. It has a mostly planar shear plane and reaches a total length of about 400 m, of which at least 150 m represents an accumulation deposit on the lake bottom, as can be identified from the October 2003 bathymetric measurements (URGH (2003b): Informe técnico: levantamiento batimetrico y topográfico de la laguna Palcacocha (in Spanish). ANA, p 6). The activity of the debris flows persists since 2004 (Emmer et al. 2014). It has a fresh-looking accumulation and a very steep and incised source area with a permanent spring. The spring is at the contact between moraine sediments and a bedrock outcrop (Fig. 5a) and has been detected repeatedly during our fieldwork in dry periods and thus is probably permanent. Another compound landslide was identified just southwest of the active debris flow (5 on Fig. 4). It consists of a smaller, secondary landslide (5a on Fig. 4), which rests on a steeply inclined slope formed by the head of a deeper and larger landslide. Both of these landslides were identified as potentially active. The secondary landslide has a fresh-looking 3-m-high scarp, suggesting relatively recent vertical movement. There are also two open tension cracks on its body (open to a depth of 0.8 m and up to 2 m wide). The body of the larger landslide is formed by ridges, which are elevated with respect to the area outside the landslide by up to 1 m. There are also several tension cracks generally sub-parallel to the margin of the slope (Fig. 5b). A deeper landslide (more than 30 m) with a retrogressive character (7 on Fig. 4) was identified close to the outburst channel of the lake. It is probably related to the slope oversteepening due to the incision of the outflow channel which formed, probably very quickly, during the catastrophic moraine breach in 1941. Shallow landslides dominate the inner slope of the northwest side moraine. Landslide no. 8 (Fig. 4) has a low scarp, suggesting low mobility of the slide mass or an initial stage of landslide development, which is the reason why it was classified as a potentially active landslide. The large landslide (9 on Fig. 4) is shallow, as shown by rock outcropping in its accumulation area.

### Internal structure of the potentially active landslides

A series of ERT profiles (Figs. 6 and 7) were measured to describe the subsurface environment of the potentially unstable rim of the lateral moraine. The results (Fig. 7) document major features identified during the geomorphological mapping. In particular, tension cracks on the secondary landslide (5 on Fig. 4) are clearly visible on profile no. 1 (Fig. 7), which also shows the geometry of the possible shear plane of the secondary landslide. Some of the tension cracks identified during field mapping that mark the scarp of the large, potentially active landslide are also clearly visible within its body (profiles 2 and 3 on Fig. 7). High and narrow resistivity zones (with resistivity over 50,000 Ωm) on the profile no. 5 ("t?" on Fig. 7) were not recognized during the field mapping, and their interpretation is unclear. They may represent tension

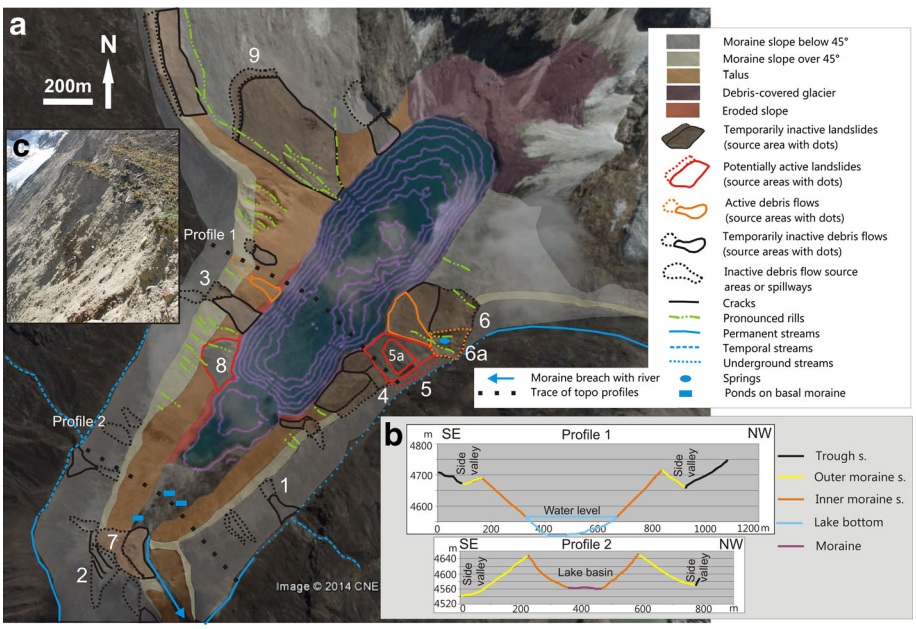


**Fig. 4** Geomorphological map (**a**) and cross profiles (**b**) of the Palcacocha Lake terminal and side moraines (*s.* slope). Topographic profiles are not exaggerated. *Inset* **c** shows body and main scarp of the secondary landslide (*2a*) (for explanations of numbers 1–9, see text). Background image is August 2013 Google Earth satellite image

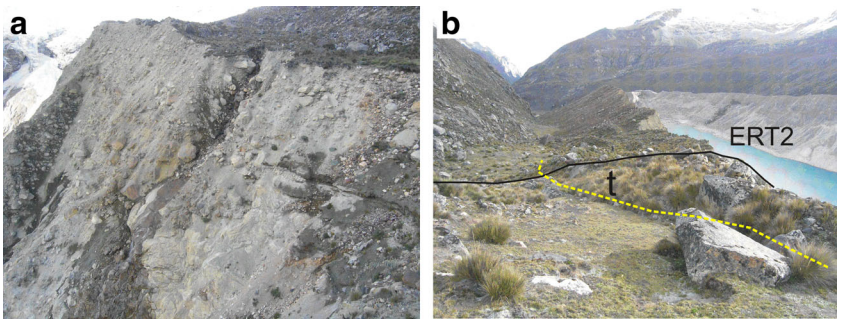


**Fig. 5** **a** Permanent spring found in the source area of the active debris flow, which is fed by a small stream as well as underground water flows bound to the contact of moraine sediment and bed rock outcrop (*lower part of the image*). **b** *Yellow line* shows tension fissure (*t*), which marks the potential scarp of the large active landslide. Trace of ERT profile no. 2 is also shown

fissures formed below the surface, which may be a precursor of possible landslide development in the future.

Extremely high resistivity readings on profile no. 1 and no. 2 ("bb" on Fig. 7) are attributed to a zone built by large boulders (diameter over 1 m), which contains numerous air-filled spaces, which, along with bedrock, have very low conductivity. A pronounced talus deposit was identified at the toe of the slope on profile no. 2. The extremely high resistivity zone identified at depth in the middle of this profile ("bb?" on Fig. 7) may represent either a buried boulder accumulation or fragments of the bedrock. The zones with low resistivity ("w" on Fig. 7) may be interpreted as relatively wet areas, where the moraine sediments are soaked by water from an underground stream. Material forming these zones may also contain a higher portion of fine particles, which would contribute to longer preservation of the wetness due to their lower hydraulic conductivity (Novotný and Klimeš 2014). These zones on profile nos. 1 and 2 do not correspond well with the topographically lowest point of the side valley. This suggests some lithological constraint on the low resistivity layers and the presence of fine-grained and presumably clay-rich materials, which exhibit quite low resistivity (e.g., 1–100 Ωm; Reynolds 2011). Lower resistivity zones on profile nos. 4 and 5 are probably not related to underground water but rather represent properties of the moraine material that better preserve moisture. This material is sharply delimited from higher resistivity regions, which are interpreted as dryer and coarser moraine material. These two contrasting materials on profile nos. 4 and 5 may also represent different generations of moraine sediments, representing complex development of the studied area.

Results of the geomorphological mapping and ERT profiles were used to estimate the volumes of the mapped landslides. The estimated volume of the secondary landslide (5a on Fig. 4) is 30,600 $m^3$, assuming 8 m as an average depth of the potentially sliding plane. Many uncertainties are involved in estimating the volume of the larger potentially active landslide, due to its more irregular shape and the possibility that it continues below the lake surface. We estimate the volume of the potential landslide to be about 630,000 $m^3$, assuming that the average potentially sliding

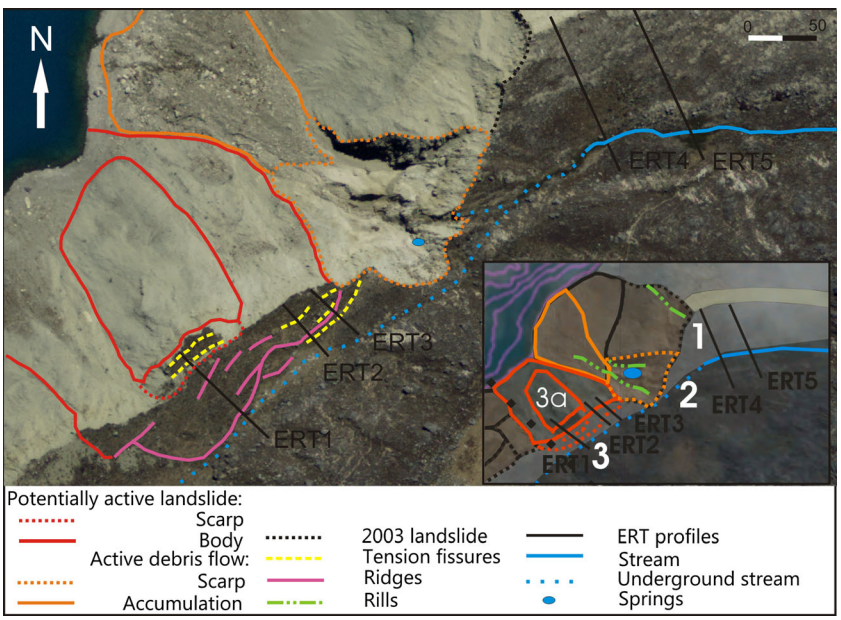


**Fig. 6** Detailed view of the potentially active landslides and ERT survey profiles, which 0 m is always on their NW end at the edge of the outer moraine slope. *Inset* shows respective portion of the geomorphological map on Fig. 4 (background image is an orthophotograph provided by ANA)

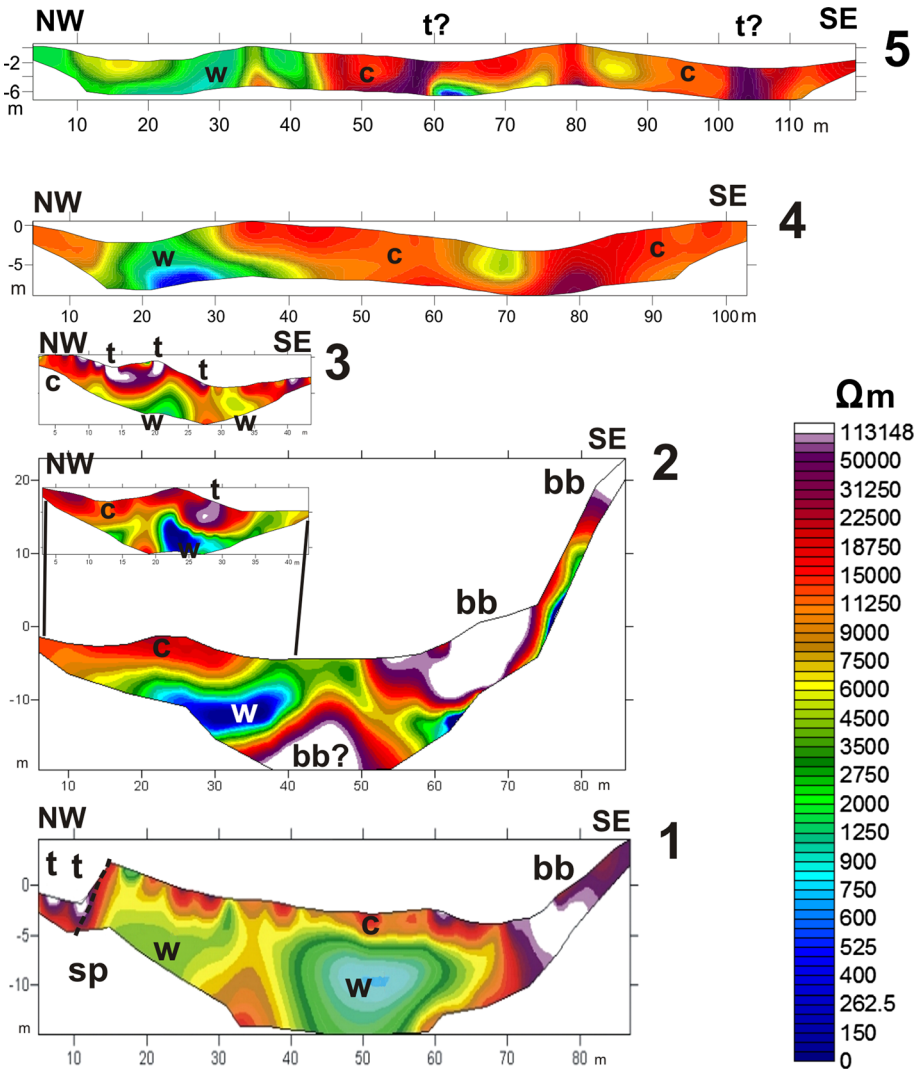


**Fig. 7** Electric resistivity tomography profiles constructed in direction along slope (*1–3*) and across slope (*4* and *5*), *sp* possible sliding plane of secondary landslide, *t* tension fissures, *c* relatively drier and coarse moraine material, *w* moraine sediment with higher water content and also probably with finer particles, *bb* large boulders with opened spaces among them and bedrock; *question mark* indicates features, which were not verified in a field and are only hypothesized

body depth was 20 m and that the landslide did not extend below the lake water level.

### Satellite SAR interferometry

The ENVISAT ASAR and ALOS PALSAR PSI displacement rates were plotted on the maps with selected geomorphological features on Fig. 8. Negative values (red colors) indicate an increase in the distance from target to satellite, i.e., a lowering of the surface. On the northwest-facing side of the valley, ENVISAT ASAR PSI results (Fig. 8a) indicate stability (i.e., displacement values below 2 mm year$^{-1}$) for large sections of the slope above the lake and movements with a rate of a few millimeter per year near the moraine crest above the temporarily inactive landslide (4 on Fig. 8a). Because, in the field, this area shows no cracks or scarps related to possible future sliding, the PSI signal might be related to the movement of superficial material. ALOS PALSAR PSI results (Fig. 8b) have a larger noise than results based on ENVISAT ASAR, because of the smaller number of acquisitions available and the larger wavelength. Nevertheless, the coverage with valid information is much larger, confirming past interferometric studies (Strozzi et al. 2005) that found that more spatially complete information can be generally found with L-band with respect to C-band. In addition, ALOS PALSAR images were acquired with a larger incidence angle than ENVISAT ASAR ones (~35° vs. ~23°), and therefore, areas masked by layover and shadow are smaller, resulting in a better coverage with valid points on both sides of the valley. ALOS PALSAR PSI results (Fig. 8b) of the ascending orbit indicate stability (i.e., displacement values below 5 mm year$^{-1}$) for large sections of the slopes above the lake and a few sectors with displacement rates approaching 10 mm year$^{-1}$. One of these sectors on the southeast moraine corresponds to the potentially active landslide detected on the geomorphological map (5 on Fig. 8b). Other areas with displacement rates slightly below 10 mm per year were identified on or close to a temporarily inactive landslide (4 on Fig. 8b), close to the terminus of the lake (10 on Fig. 8b), and between two temporarily inactive landslides on the southeast-

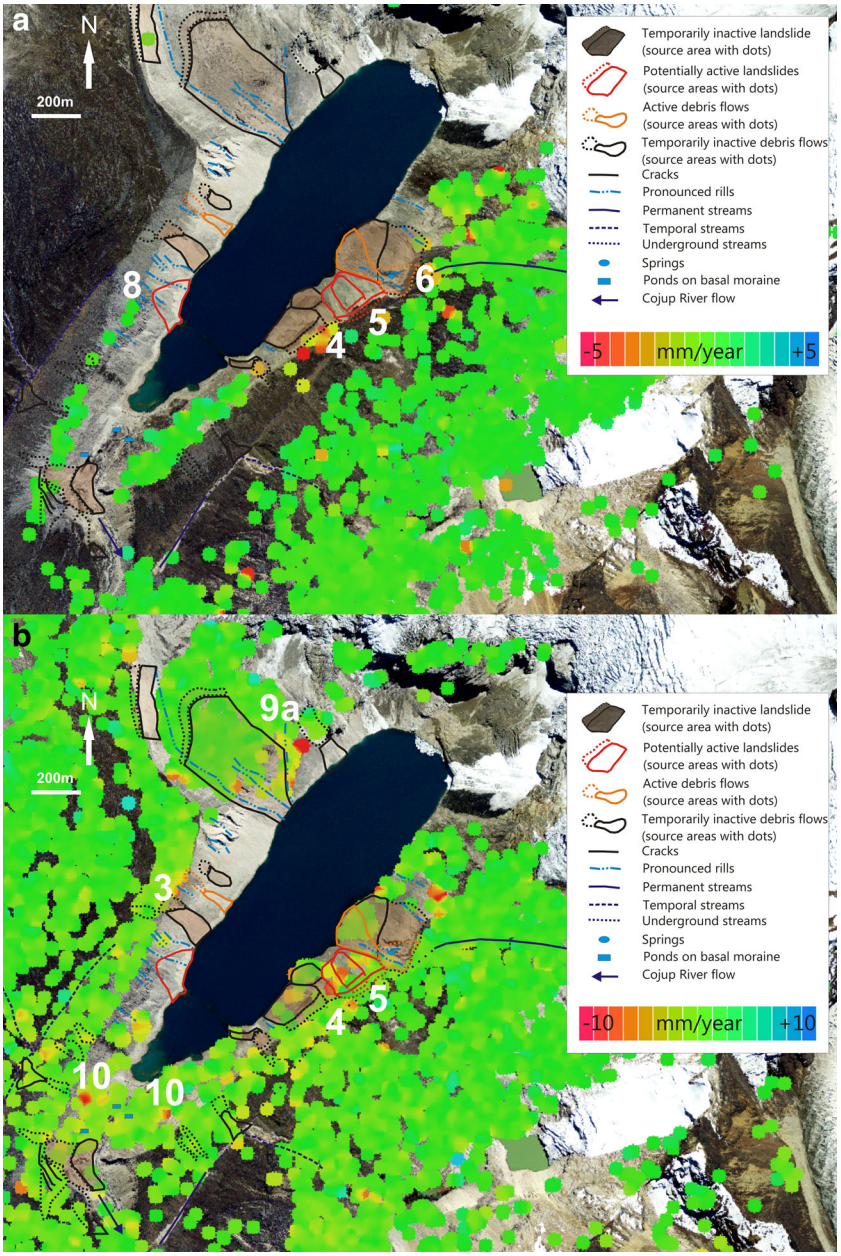


**Fig. 8** Results of ENVISAT ASAR (**a**) and ALOS PALSAR (**b**) PSI displacement rates are shown along landslides from geomorphological map. Negative values (*red colors*) indicate an increase in the distance from target to satellite, i.e., a lowering of the surface (for explanations of numbers 1–10, see the text). Background image is August 2013 Google Earth satellite image

facing moraine slopes (9a on Fig. 8b). In the cases 4, 9a, and 10 (Fig. 8b), high-activity areas are on places where mainly movement of superficial material can occur, often related to the pronounced rills. The PSI results do not indicate significant movements along any of the cracks or scarps found in the field related to possible future sliding (5 on Fig. 8). The confirmation of no activity along geomorphologically identified scarps and potential scarps of landslides is very useful information with respect to their hazard assessment.

Areas without PSI points are identified not only for water, snow/ice, and layover/shadows, as expected, but also on many parts of the moraine. For instance, on the scarp of the recently active landslide (5 and 6 on Fig. 8a), no ENVISAT ASAR PSI points were detected, and on large sections of the moraine on the northwest side of the lake, there are no ALOS PALSAR PSI points (3 and 8 on Fig. 8). Because the presence of snow cover or vegetation can be excluded, decorrelation on PSI results might indicate the presence of movements more rapid than a few centimeters per year. In these cases, interpretation of single SAR interferograms can be useful for a more complete picture of the displacements. Using differential InSAR (DInSAR) analysis, we identified zones with displacement rates of 100 to 500 mm year$^{-1}$ classified according to Barboux et al. (2014, see Online Resource 1). Three such zones with major coherent phase signals were detected between 2007 and

2010 over the northwest side of the lake (yellow zones on Fig. 9). Field investigation suggested that, in some cases, displacements reflected mainly processes that do not generate landslide morphology (zone 11 on Fig. 9) and are represented by near continuous down-slope transport of superficial sediments and their accumulation on the talus of the inner slope. In other places (zone 12 on Fig. 9), it corresponded well to a shallow landslide identified during geomorphological mapping, and thus, it reflected its movement activity (compare with 8 on Fig. 4). Another major signal was detected in 1998 on the northwest-facing slope of the lake (13 on Fig. 9) with ERS SAR data over the potentially active landslides and landslide from 2003. It could be considered as a possible movement precursor signal for the 2003 landslide. After 2003, ENVISAT ASAR interferograms taken over 35 days or more show decorrelation in this area, which was probably caused by major activity of this landslide following its occurrence in March 2003. Unfortunately, the 11-day TerraSAR-X interferograms, which are characterized by a very high resolution of 3 m and could have been very useful for our investigations (Notti et al. 2010), had a very large baseline of more than 500 m and were not useful for our study. Over the area of the 2003 landslide, the TerraSAR-X interferogram seemed to be decorrelated as well. In yearly DInSAR interferograms, decorrelation was observed for large areas of the moraine (green zones on Fig. 9). Remaining patches of snow or snow avalanches could have caused the decorrelation detected close to the glacier terminus. But, in other areas (zones 14 and 15 on Fig. 9), mobility of superficial material and landslide activity may be responsible for the signal decorrelation.

### Slope stability calculations of potentially active landslides

A factor of safety was calculated using a fully specified slip surface, as well as a slip surface defined by calculation as kinematically best suited for the development of the studied landslide. These surfaces were almost identical (Fig. 3). Calculations of the factor of safety (Fs) considering the strength in a critical state for dry material resulted in values below the limiting state—Fs = 0.829. This was not surprising, as the values of the angle of internal friction were lower than the actual slope dip of the modeled profile (Novotný and Klimeš 2014). Therefore, we tested the slope stability by considering the peak strength, which probably governed the recent slope stability conditions. The calculated Fs of the dry, cohesionless, and homogeneous moraine material fraction of up to 22-mm grains was very close to 1 (Table 2), which was unrealistic considering the recent steep topography. Therefore, we introduced an apparent cohesion into the calculations, which accounted for the stabilizing effects of large boulders and their sedimentation characteristics, as suggested by previous work (Novotný and Klimeš 2014). To obtain, a Fs = 1.1 (above the stability threshold) of dry material required using an effective cohesion of 10 or 12 kPa (Table 2). It showed for the dry material that the slope was stable, but still very sensitive to any factors possibly lowering its stability (e.g., water saturation). Sensitivity calculations for varying degrees of water saturation were carried out. For example, the factor of safety was close to the limiting value 1 in the model case when 10 % of material above the slip surface was fully saturated. A further increase of water content above the slip surface mathematically reduces the factor of safety to below 1. For example, in the model case, when 50 % of material above the slip surface was fully saturated, the factor of safety was reduced to 0.65, for which the slope was very unstable (Table 2).

The effects of seismicity are an important destabilizing factor for slopes. Since the study area could be subject to earthquakes, we

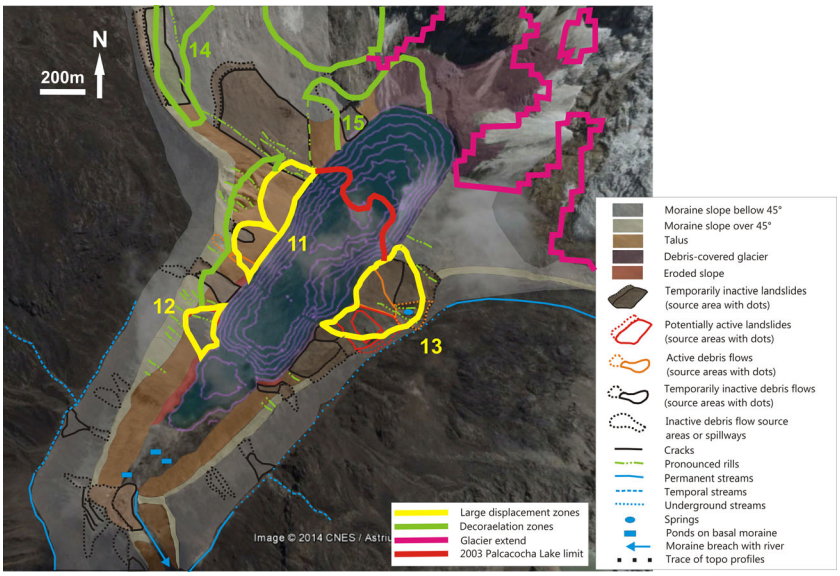


**Fig. 9** Results of the DInSAR analysis interpretation (for additional information, see Online Resource 1). *Yellow outlines* define zones with detected movement rates of 10–50 cm year$^{-1}$ with years when the major displacements were detected. Areas on the orographic right slopes of the Palcacocha Lake were detected with ALOS PALSAR image pairs with a time interval of 46 days and ENVISAR ASAR image pairs with a time interval of 35 days. The area on the left moraine slope was identified using ERS SAR image pairs with 35-day interval. Areas with decorrelation observed in yearly or monthly DInSAR interferograms are shown by *green lines*. The signal decorrelation could be caused by snow patches near the glacier or by large mobility of superficial material or landslide activity. Extent of the Palcacocha Lake in 2003 is shown by *red outline*. Glacier extents from Randolph Glacier Inventory Version 4.0 (Arendt et al. 2014) are shown by *pink lines*. Background image is August 2013 Google Earth satellite image

**Table 2** Factor of safety calculated using peak strength

| Water content | Factor of safety | |
|---|---|---|
| | $c = 0$ | $c = 10–12$ kPa |
| Dry | 0.998/0.972 | 1.089–1.107 |
| 10 % of material above slip surface is fully saturated[b] | – | 0.998–1.015 |
| 50 % of material above slip surface is fully saturated[a] | – | 0.640–0.657 |

[a] Water content of the material above sliding surface was characterized by pore pressure coefficient $r_u = 0.25$

[b] Water content of the material above sliding surface was characterized by pore pressure coefficient $r_u = 0.05$

performed a series of calculations showing the effects of seismicity on slope stability under different water saturation conditions (Fig. 10). They show the high sensitivity of the factor of safety to the seismic $k_h$ coefficient. In the case of a dry slope with increased cohesion ($c = 10–12$ kPa), Fs drops to 1 when a $k_h$ of only 0.05 is applied. This value of $k_h$ corresponds to earthquake magnitudes from Mw 5 to Mw 7 (Idriss 1985; STN 730036).

Ice support of the adjacent slopes is a well-recognized factor contributing to slope stability, and increased slope movement is often related to glacier retreat (Evans and Clague 1994; Holm et al. 2004; Hugenholtz et al. 2008; Oppikofer et al. 2008). Therefore, we calculated a theoretical height above the recent water level of the glacier within the terminal moraine, which would increase the landslide stability to over a threshold value of Fs = 1. With increasing ice thickness, slope height above the ice decreased, which has a major effect on slope stability increase. From a variety of possible slope stability conditions, we decided to present results of two scenarios representing possible worst-case scenarios for the studied slope. The apparent cohesion was always set to 12 kPa. The first scenario was defined by $r_u = 0.05$ (10 % of material above slip surface was fully saturated) and $k_h = 0.1$ (approximately Mw 6–7, Idriss 1985; STN 730036). The second scenario had $r_u = 0.25$ (50 % of material above slip surface was fully saturated) and $k_h = 0$ (no seismicity). The first scenario with applied seismicity and less water above the slip surface (scenario 1 on Fig. 11) showed that the factor of safety reached the threshold value when the slope height above the glacier surface was 35 m or less (corresponding to a glacier thickness of 95 m above the recent lake water level at 4562 m a.s.l.). Calculations which applied a greater water portion above the slip surface and no seismicity (scenario 2 on Fig. 11) showed that the slope stability reached the Fs = 1 when the slope height was only 25 m, corresponding to a glacier thickness of 110 m. A significant re-advance of the glacier at Palcacocha Lake can be excluded; nevertheless, these sensitivity calculations indicated that unstable conditions in the moraine slopes of Palcacocha Lake probably existed already during periods of ice-surface lowering, when the glacier was still present within the studied moraines.

### Hydrodynamic model of landslide-induced impact waves

Results of the Iber model provided a relative measure of the potential of a landslide to trigger impact waves of a specific size related to landslides of specific dimensions (Table 3). Landslide volume and impact wave height triggered by the 2003 compound landslide (1 on Fig. 4) were used for back calculations, enabling the best-fit estimation of landslide velocity entering the lake to be 7 m $s^{-1}$. Subsequently, the potentially active compound landslides were modeled (Table 3), showing that the impact wave caused by the main potentially active landslide (5 on Fig. 4) could reach 8 m in height, with a maximum flow of 29,400 $m^3$ $s^{-1}$ before reaching the reinforced dam. Its magnitude would be very similar to the wave triggered by the 2003 compound landslide. The calculated impact wave caused by the smaller, secondary landslide of the potentially active compound landslide (2a on Fig. 4) would not overcome the existing artificial dams, as its maximum height was only 1 m, while the dam freeboard is 7 m. This result reflected the small estimated volume of the secondary landslide. The height similarity between impact waves caused by the 2003 compound

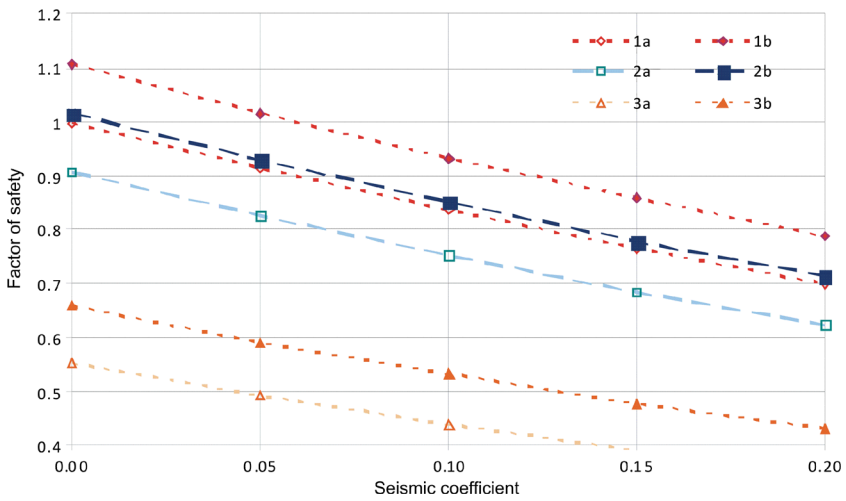


**Fig. 10** Changes of the factor of safety ($F_s$, $y$-axis) due to increasing seismic loading ($k_h$, $x$-axis), 1a—dry with $c = 0$ kPa, 1b—dry with $c = 12$ kPa, 2a—10 % of material above slip surface is fully saturated with $c = 0$ kPa, 2b—10 % of material above slip surface is fully saturated with $c = 12$ kPa, 3a—50 % of material above slip surface is fully saturated with $c = 0$ kPa, 3b—50 % of material above slip surface is fully saturated with $c = 12$ kPa

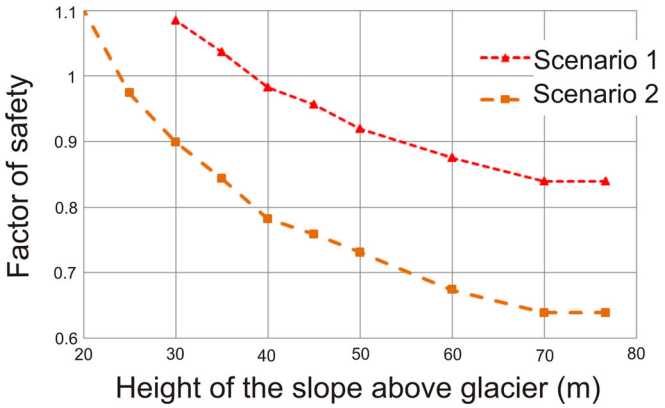


**Fig. 11** Changes of the factor of safety due to increasing height of the glacier, scenario 1—$c = 12$ kPa, $r_u = 0.05$ (10 % of material above slip surface is fully saturated), and $k_h = 0.1$; scenario 2—$c = 12$ kPa, $r_u = 0.25$ (50 % of material above slip surface is fully saturated), and $k_h = 0$

landslide and the potential failure of the newly described landslide suggested that also a glacial lake outburst flood due to the landslide failure would have a similar magnitude to the one in 2003. In this case, the outburst flood effects were only minor and restricted to minor damage to the drinking water treatment facilities located very close to the Cojup River. The ongoing drainage works, using siphons at Palcacocha Lake, might even be sufficient to prevent a spillover of such a small-magnitude outburst flood, since the lake level (field visit in April 2015) was about 3.4 m below the artificial outlet originally designed to keep the lake water level at 4562 m a.s.l.

## Discussion

### Slope stability and landslide occurrence

Debuttressing of debris-mantled slopes (i.e., removal of their toe support) significantly contributes to landslide occurrence (Haeberli et al. 1997; Hugenholtz et al. 2008) but may be compensated for by post-glacial slope development. In this case, formation of talus has reduced the slope angle from about 55° in the upper part of the inner moraine slope to about 35° at its toe at Palcacocha Lake. Also, our slope stability calculations showed that significant ice buildup would be necessary to push the slope stability above the critical threshold of the factor of safety. In the scenario in which only water infiltration was considered as the destabilizing factor (i.e., 50 % of material above slip surface was fully saturated), the stability of the modeled slope dropped below Fs = 1 (Fig. 11) when the slope height above the glacier surface was more than 25 m. In other words, our calculation results showed that when the glacier thickness dropped to below 110 m or less above the recent water level, the slope started to be highly unstable under the specified hydrological and recent morphological conditions. The low slope stability was confirmed by the landslide mapping, which identified repeated and localized landslide activity, mostly on the northwest-facing moraine slope, as well as PSI SAR data analysis showing high decorellation explained by superficial movements exceeding a few centimeter per year. The later process does not include landsliding defined by development of sliding planes and landslide forms, but rather individual movements of large boulders or removal of material by sheet and rill erosion on steep slopes. On the other hand, the fact that landslide occurrence in the steep part of the moraine slopes was not very frequent, at least based on available landslide inventory data, and the recorded recent activity was spatially limited suggests that landslide initiation was strongly governed by specific slope stability conditions (e.g., buried ice, concentrated water flow, site-specific properties of moraine material) as well as by the occurrence of specific triggering events (e.g., precipitation or earthquakes). Comparable results for landslide distribution stimulated regional-scale investigation of the role of post-Little Ice Age (LIA) Neoglacial retreat on landslide activity in British Columbia (Holm et al. 2004). This study suggests that complex landslide occurrence patterns are determined by the type of material, relief morphology, and availability of suitable sediments, which is affected by glacier aggradation and removal processes.

The slope stability calculations were done with good knowledge of the basic mechanical and strength properties of the modeled material, which was sampled directly from the scarp area of the potentially active landslide. The large shear box tests performed on the landslide material allowed us to define peak shear strengths as function of normal stresses, representing different depths below landslide surface. This information was used in the slope stability calculations. Despite such detailed input data, the calculation results need to be carefully evaluated, since some additional parameters still could only be estimated. Among them were the effects of large block wedging (Novotný and Klimeš 2014) or moraine sedimentation fabrics that tend to parallel the outer moraine slope surface (Lucas and Sass 2011) and which were also confirmed by field observations at the Palcacocha Lake moraine. Shear planes on the inner slopes have to cut across this

**Table 3** Characteristics of the main input parameters and results of the Iber hydrodynamic model

| | 2003 Compound landslide | Potentially active compound landslide | |
|---|---|---|---|
| | | Main landslide | Secondary landslide |
| Landslide volume ($m^3$) | 756,000 | 630,000 | 30,600 |
| Landslide depth (m) | 17.2 | 20 | 8 |
| $Q_{max}$ ($m^3\ s^{-1}$) | *23,000* | *29,400* | *2500* |
| $W_h$ ($m$) | *8* | *8* | *1* |

The results of the Iber hydrodynamic model are in italic. Landslide velocity at entry to the lake was estimated to 7 m $s^{-1}$

$w_h$ maximum height of the impact wave before reaching the dam crest, $Q_{max}$ maximal flow of the highest modeled wave before reaching the dam crest

sedimentation structure, where rock blocks oriented parallel to the outer slope may cause apparent cohesion of the moraine material. Another factor which could increase the stability of the moraine slopes under natural conditions was suction (compare with Springman et al. 2003). Its action at the study site was witnessed during field work on wet moraine material at shallow depths (already 0.3 m under the surface) even during dry season. All these factors were accounted in the calculations by introducing an apparent cohesion of 10–12 kPa. Nevertheless, there is uncertainty in how well these additional stability factors are reflected by these values. In the case of the 2003 compound landslide, water pressure generated by the spring in the crown area was probably the factor that possibly lowered the slope stability (compare with URGH, 2003 Informe técnico: Estado situacional de la laguna Palcacocha (in Spanish). ANA, p. 19) and was not reflected in the stability calculations.

Historical and recent geomorphological mapping showed that landslides in the last 60 years occurred mainly on the southeast lateral moraine of Palcacocha Lake, close to the glacier. The strong persistence of landsliding in this location was probably caused by the availability of surface and subsurface water, which was being supplied by a small stream coming from the higher parts of rock slopes of the trough. The high water availability at this site was due to the fact that the moraine was underlain by a rock slope at relatively shallow depths (evidenced by rock outcrops seen in the active debris flow source area, Fig. 5a). Thus, this slope could be classified as a "rock-controlled slope," which represented terrain most associated with surficial landslides in areas affected by post-Little Ice Age glacier retreat (Holm et al. 2004). The importance of water saturation on triggering landsides in moraines was further supported by examples of landslides which occurred after periods of heavy precipitation (e.g., Santa Teresa, Cuzco in Klimeš et al. 2007 or Giráldez et al. 2013) or due to water seepage through lateral moraine (Cangrajanca Lake, Cordillera Huayhuash in Engel et al. 2011). Some other works do not mention this factor (e.g., Hugenholtz et al. 2008), but local slope morphology inferred from published aerial photos suggested that water concentration from slopes adjacent to the moraine could play a role in landslide mobilization.

#### SAR analysis and landslide identification

The PSI analyses of ALOS PALSAR images showed displacement rates approaching 10 mm year$^{-1}$ on the southeast lateral moraine, corresponding to the area of potentially active landslide detected on the geomorphological map (5 on Fig. 8b). Moving PSI points were nevertheless grouped over the landslide body, and no displacement was detected on the PSI over the identified scarps of the landslide described by field mapping as potentially active in the future. This could be explained by recent activity of the landslide scarp area being too small to be detected by the SAR technology (in particular, considering the unfavorable orientation of the ALOS PALSAR with respect to the slope orientation), or the possible displacements along the scarp were not captured by the available time series of ALOS PALSAR images (2007–2011). These findings, along with repeated field observations (2011–2014) which revealed no major activity, represented positive information with respect to the probability of rapid future reactivation, which was more likely to occur in cases when nearly continual deformation occurred. Field evaluation of other PSI signals detected on the moraine with both ENVISAT ASAR and ALOS PALSAR analyses attributed the deformation to movements of superficial material or to a compaction of the moraine. Two zones of major coherent phase signals detected by DInSAR interferograms on the northwest side of the moraine, with displacement rates of 10 to 50 mm year$^{-1}$ (yellow zones on Fig. 9), illustrated advantages of mutual PSI and DInSAR data interpretation. These signals were attributed to both movement of superficial materials (11 on Fig. 9) and landsliding (12, 13, 14, and 15 on Fig. 9), which showed the importance of complementing SAR interferometry with field geomorphological mapping, in particular, when the proper mechanism behind the detected displacements needed to be defined. This notion was further supported by the fact that the movements detected by the PSI as well as the DInSAR analyses generally coincided with landslide occurrence on the southeast moraine. The "precursor" role of movements detected by DInSAR analysis may be considered only if it is detected at places with favorable conditions for landslide initiation. So far, it seems that such additional conditions were limited to the March 2003 landslide (6 on Fig. 4) and its close surroundings and were not detected on the northwest moraine.

#### Glacial lake outburst floods triggered by moraine landslides

Field investigation and calculations from Palcacocha Lake, as well as experience from historical events, showed that landslides on the moraine slopes with the possibility of entering the lake could produce impact waves responsible for initiating glacial lake outburst floods. The magnitudes of these outburst floods seemed to be limited, and similar results obtained for the 2003 event as well as the new landslides scenarios suggested that floods with only a small extent would be produced by the studied moraine landslides under the specified conditions (note that the actual water level was 3.4 m lower than the one used in the hydrodynamic model). These contain the landslide volume and velocity at the entry to the lake, as well as shape of the lake basin and location of the material entry into the lake. The reliability of the resulting model depended on how reliably determined these input variables were. The shape of the lake basin and location of the material entering into the lake were reliably described by available topographic data and field mapping. Higher uncertainty was related to estimation of the landslide volume determined from the landslide depth, which was reliably known only along the ERT profile. This, however, is a large improvement compared to other impact wave models (Schneider et al. 2014), in which the volume was estimated by experts using remotely sensed data. The velocity at the entry into the lake was determined by the best-fit back calculation from the 2003 landslide event still providing reliable results.

Simulation of the impact of an ice avalanche (Somos-Valenzuela et al. 2014), with a volume of $5 \times 10^5$ m$^3$ comparable to our scenarios (Table 3), with the comparable higher velocity of 20 m s$^{-1}$ entering Palcacocha Lake at its very beginning and travelling along its longitudinal axis, results in an estimated

maximum height of the impact wave of 9 m. In this case, the volume of the material was set arbitrary, using literature values. When the ice avalanche volume is increased to $1 \times 10^6$ $m^3$, the impact wave more than doubles to 21 m. The different conditions of the ice avalanche and landslide simulations, as well as the significant increase of the impact wave height when increasing the total volume of the ice avalanche, suggested that the relatively small volume of the avalanche and landslide material was responsible for similar impact wave heights of 8 and 9 m respectively. While in the case of the ice and ice/rock avalanches coming from the glaciated parts of the mountain ridges (Schneider et al. 2014), it is very difficult to reliably estimate possible volumes of the past as well as future avalanches, volumes of the landslides from the moraine slopes can be constrained more objectively, as shown in this study. Even without detailed field information, the possible variability in the landslide volumes was highly constrained by the moraine morphology and total volume of available material. Therefore, we assumed that glacial lake outburst floods resulting from landslides in moraines will be probably smaller than outburst floods triggered by other mass movements (Fig. 1), which may involve much larger volumes of material entering the lake at higher velocities and at a different angle with respect to the lake longitudinal axis. This assumption has direct implications for glacial lake outburst flood hazard assessment. Considering that the calculated wave heights correspond to about the height of the dam above the artificial outlet channel, the progress of ongoing measures to lower lake water level has an immediate effect on the potential hazard. In April 2015, the lake level was already lowered to about 3.4 m below the original level, which, according to the hydrodynamic impact wave modeling, would already be sufficient to prevent a spillover of the dam for both the 2003 landslide and the future landslides.

Examples of documented glacial lake outburst floods triggered by landslides from inner moraine slopes listed in the caption of Fig. 1 suggest that Palcacocha Lake is not the only lake in the Cordillera Blanca that has favorable conditions to trigger outburst floods by moraine landslides. So far, there has been no detailed regional evaluation of moraine slope stability of glacial lakes focusing on this phenomenon, but there are several well-known examples of lakes susceptible to similar glacial lake outburst floods within the Cordillera Blanca region (e.g., Jancarurish—8° 51′ 32″ S, 77° 40′ 22″ W; Arhueycocha—8° 53′ 17″ S, 77° 37′ 44″ W; Allicocha—9° 15′ 03″ S, 77° 27′ 33″ W; Pag Pag—9° 04′ 04″ S, 77° 33′ 20″ W; Tullpacocha—9° 25′ 10″ S, 77° 20′ 27″ W). Landslides similar to those described in this study may have occurred at these other lakes, but if they triggered only small magnitude outburst floods, these may not have been recorded. Despite the presented evidence and assumptions about glacial lake outburst flood magnitudes, it could be very dangerous to underestimate future outburst floods triggered by landslides from moraines. Large-volume or high-velocity landslides from moraines on sites with different morphological and geological settings could initiate waves capable of even breaching the moraine dams, possibly causing large glacial lake outburst floods. Climate-driven environmental changes may critically affect stabilities of slopes above glacial lakes, possibly triggering large moraine landslides. Thus, continuous remote sensing and field-based monitoring and related hazard assessments (e.g., Reynolds 2003; Klimeš 2012; Emmer and Vilímek 2014) are important steps in risk management and effective mitigation of glacial lake outburst flood hazards. They should also consider the impacts of ongoing environmental change (e.g., glacier retreat, permafrost degradation, and associated slope response, mainly water infiltration to the lateral moraines). Structural measures can help to decreasing the susceptibility of moraine-dammed lakes to produce outburst floods caused by overtopping or even breaching of the moraine dams. Effective mitigation strategies should increase dam freeboard and reinforce the lake outlet, i.e., especially creating artificial dams, in combination with open cuts or digging outflow tunnels (Emmer et al. 2016). The majority of large moraine-dammed lakes of the Cordillera Blanca have some of these structural measures; nevertheless, the 2003 outburst flood from Palcacocha Lake showed that floods resulting from moraine sliding into the lake may occur in already remediated lakes, which thus should not be excluded from continuous hazard re-assessment. Such mitigation works typically significantly reduce the hazard potential but do not reduce it to zero. As an alternative to construction works, other measures can be applied to lower the risks of floods, by decreasing the vulnerability of the potentially affected population, i.e., improving their preparedness and response in the event of an outburst. Examples for such so-called non-structural measures are early warning systems (EWSs) to alert the population in case of a flood. In the Cordillera Blanca, such a EWS has recently been successfully implemented at Lake 513 (Frey et al. 2014), which also experienced a glacial lake outburst flood in 2010, despite structural mitigation measures (Klimeš et al. 2014; Schneider et al. 2014).

## Conclusions

Occurrences of landslides on inner slopes of lateral moraines as possible triggers of glacial lake outburst floods from Palcacocha Lake have been investigated. Detailed field morphological and geophysical data are required to reliably assess volumes of landslides causing impact waves. Proper estimation of the volume of material entering the lake is important to substantially increase the reliability of results of hydrodynamic wave modeling. Local topography is also important in the slope stability calculations that show that slopes of the lateral moraines are close to the stability threshold and are sensitive mainly to the water content. Nevertheless, the calculations leave open questions about stabilizing factors, which ensure the temporal stability of the moraine slopes, even during potential triggering events of high intensity (e.g., high-magnitude earthquakes). The presence of glaciers is often regarded as a stabilizing factor for adjacent slopes. Parametric stability calculations showed that considerable thickness of glacier support of the slope is required to increase its stability above the threshold limit under recent morphological conditions. This suggests that large portions of moraine slopes were highly unstable even during earlier periods of glacier thinning. This finding, along with the documented strong spatial persistence of landslides on the Palcacocha lateral moraine,

shows that site-specific conditions related to water saturation are important factors for landslide occurrence in the inner slopes of exposed moraines.

Back calculation of the impact waves triggered by a historical landslide and landslide scenarios based on field evidence and slope stability calculations suggest similar magnitudes for past and potential future impact waves. Subsequent comparison with the 2003 flood suggests that floods of only small extent may be produced by the studied landslides in moraine under the specified conditions of Palcacocha Lake. Ongoing efforts to lower the lake level and increase the dam freeboard may already be sufficient to prevent a spillover at the dam in case of a landslide impact. Findings suggest that floods triggered by landslides in moraines are smaller than floods caused by other slope processes (e.g., ice/rock avalanches) due to the generally smaller entry velocities and volumes of landslides from the lateral moraines. This assumption has to be critically evaluated against site-specific conditions at a given lake (e.g., possible dam breach) and any possible environmental changes that may cause increased water content in the moraine material. Additional water input into the moraines may mobilize larger volumes, possibly causing higher impact waves and thus posing a higher glacial lake outburst flood hazard.

## Acknowledgments

The authors wish to acknowledge the financial support provided by the Czech Science Foundation (Grant No. P209/11/1000), Grant Agency of Charles University (GAUK project no. 70 413; GAUK project no. 730 216), the European Space Agency (S:GLA:MO project), and the Swiss Agency for Development and Cooperation (SDC) (Proyecto Glaciares). This work was carried out thanks to the support of the long-term conceptual development research organisation RVO: 67985891. ERS and ENVISAT SAR data courtesy of C1F.6504, © ESA. ALOS PALSAR © JAXA. TERRASAR-X data courtesy HYD0562, © DLR. We thank John M. Reynolds for a very detailed and helpful review as well as Matt Rowberry and Christian Huggel for their valuable comments.

## References

Arendt A, Bliss A, Bolch T, Cogley JG, Gardner AS, Hagen JO, Hock R, Huss M, Kaser G, Kienholz C, Pfeffer WT, Moholdt G, Paul F, Radić V, Andreassen L, Bajracharya S, Barrand N, Beedle M, Berthier E, Bhambri R, Brown I, Burgess E, Burgess D, Cawkwell F, Chinn T, Copland L, Davies B, De Angelis H, Dolgova E, Filbert K, Forester R, Fountain A, Frey H, Giffen B, Glasser N, Gurney S, Hagg W, Hall D, Haritashya UK, Hartmann G, Helm C, Herreid S, Howat I, Kapustin G, Khromova T, König M, Kohler J, Kriegel D, Kutuzov S, Lavrentiev I, LeBris R, Lund J, Manley W, Mayer C, Miles ES, Li X, Menounos B, Mercer A, Mölg N, Mool P, Nosenko G, Negrete A, Nuth C, Pettersson R, Racoviteanu A, Ranzi R, Rastner P, Rau F, Raup B, Rich J, Rott H, Schneider C, Seliverstov Y, Sharp M, Sigurðsson O, Stokes C, Wheate R, Winsvold S, Wolken G, Wyatt F, Zheltyhina N (2014) Randolph Glacier Inventory—a dataset of global glacier outlines: version 4.0. Global Land Ice Measurements from Space, Boulder Colorado, Digital Media

Bamler R, Hartl P (1998) Synthetic aperture radar interferometry. Inverse Probl 14:R1-R54. doi:10.1088/0266-5611/14/4/001

Barboux C, Delaloye R, Lambiel C (2014) Inventorying slope movements in an Alpine environment using DinSAR. Earth Surf Process Landf 39:2087–2099. doi:10.1002/esp.3603

Bareither CA, Edil TB, Mickelson DM (2008) Geological and physical factors affecting the friction angle of compacted sands. J Geotech Geoenvironmental Eng 134:1476–1489

Beló M, D'Agata C, Smiraglia C, Plefini M (2006) Ice core moraine collapse at Froni Glacier (Italian Alps): a case of tourist risk. Geophys Res Abstr 8 (08361)

Bolton MD (1986) The strength and dilatancy of sands. Géotechnique 36:65–78

Carey M (2010) In the shadow of melting glaciers: climate change and Andean society. Oxford University Press, p 288

Carey M (2005) Living and dying with glaciers: people's historical vulnerability to avalanches 524 and outburst floods in Peru. Global Planet Change 47(2–4):122–134

Cigna F, Bianchini S, Casagli N (2012) How to assess landslide activity and intensity with persistent scatterer interferometry (PSI): the PSI-based matrix approach. Landslides. doi:10.1007/s10346-012-0335-7

Costa JE, Schuster RL (1988) The formation and failure of natural dams. Geological Society of America Bulletin 100(7):1054–1068. doi:10.1130/0016-7606(1988)100<1054:TFAFON>2.3.CO;2

Crosetto M, Monserrat O, Bremmer C, Hanssen R, Capes R, Marsh S (2009) Ground motion monitoring using SAR interferometry: quality assessment. Eur Geol 26:12–15

Emmer A, Vilímek V, Klimeš J, Cochachin A (2014) Glacier retreat, lakes development and associated natural hazards in Cordillera Blanca, Peru. In: Shan W, Guo Y, Wang F, Marui H, Strom A (eds) Landslides in cold regions in the context of climate change, Springer, pp 231–252

Emmer A, Cochachin A (2013) The causes and mechanisms of moraine-dammed lake failures in the Cordillera Blanca, North American Cordillera and Himalayas. AUC Geograph 48:5–15

Emmer A, Vilímek V (2014) New method for assessing the susceptibility of glacial lakes to the outburst floods in the Cordillera Blanca, Peru. Hydrol Earth Syst Sc 18:3461–3479. doi:10.5194/hess-18-3461-2014

Emmer A, Loarte EC, Klimeš J, Vilímek V (2015) Recent evolution and degradation of the bent Jatunraju glacier (Cordillera Blanca, Peru). Geomorphology 228:345–355

Emmer A, Vilímek V, Zapata ML (2016) Hazard mitigation of glacial lake outburst floods in the Cordillera Blanca (Peru): the effectiveness of remedial works. J Flood Risk Manage, not yet assigned to an issue. doi:10.1111/jfr3.12241

Engel Z, Č esák J, Rios Escobar V (2011) Rainfall-related debris flows in Carhuacocha Valley, Cordillera Huayhuash, Peru. Landslides 8:269–278

Evans SG, Clague JJ (1994) Recent climatic change and catastrophic geomorphic processes in mountain environments. Geomorphology 10:107–128

Farina P, Colombo D, Fumagalli A, Marks F, Moretti S (2006) Permanent scatterers for landslide investigations: outcomes from the ESA-SLAM project. Eng Geol 88:200–217

Fischer T, Lentschke J, Küfmann C, Haas F, Baume O, Becht M, Schröder H (2013) High-mountainous permafrost under continental-climatic conditions: actual results of different mapping methods and an empirical-statistical modeling approach for the Northern Tien Shan. Geoph Res Abs 15:EGU2013–13074

Frey H, García-Hernández J, Huggel C, Schneider D, Rohrer M, Gonzales Alfaro C, Muñoz Asmat R, Price Rios K, Meza Román L, Cochachin Rapre A, Masias Chacon P (2014) An early warning system for lake outburst floods of the Laguna 513, Cordillera Blanca, Peru. In: Proceedings of the International Conference on the Analysis and Management of Changing Risks for Natural Hazards. 18–19 November 2014, Padua, Italy

Giráldez C, Choquevilca W, Fernández F, Frey H, García J, Haeberli W, Huggel C, Ludena S, Rohrer M, Suarez W (2013) Large mass movements related to deglaciation effects in southern Peru (Cusco). Geoph Res Abs 15:EGU2013–8183

Haeberli W, Wegmann M, Vonder Muhll D (1997) Slope stability problems related to glacier shrinkage and permafrost degradation in the Alps. Ecologae Geologicae Helvetiae 90:407–414

Holm K, Bovis M, Jakob M (2004) The landslide response of alpine basins to post-Little Ice Age glacial thinning and retreat in southwestern British Columbia. Geomorphology 57:201–216

Hölbling D, Füreder P, Antolini F, Cigna F, Casagli N, Lang S (2012) A semi-automated object-based approach for landslide detection validated by persistent scatterer interferometry measures and landslide inventories. Remote Sens 4:1310–1336

Hubbard B, Heald A, Reynolds JM, Quincey D, Richardson SD, Zapata-Luyo M, Santillan-Portilla N, Hambrey MJ (2005) Impact of a rock avalanche on a moraine-dammed proglacial lake: Laguna Safuna Alta, Cordillera Blanca, Peru. Earth Surf Process Landf 30:1251–1264

Hugenholtz CH, Moorman BJ, Barlow J, Wainstein PA (2008) Large-scale moraine deformation at the Athabasca Glacier, Jasper National Park, Alberta, Canada. Landslides 5:251–260

Huggel C, Gruber S, Korup O (2013) Landslide hazards and climate change in high mountains. In: Shroder J, James LA, Harden CP, Clague JJ, Shroder J (eds) Treatise on geomorphology. Academic Press, San Diego, pp 288–301

Iber (2010) Two-dimensional modeling of free surface shallow water flow, Hydraulic reference manual, Iber v1.0. http://www.iberaula.es/web/index.php. Accessed 20 January 2014

Idris IM (1985): Earthquake ground motions. In: EERI Course on "Strong ground motion—seismic analysis, Design and code issues," April 10th 1987, Pasadena, California

Instituto Nacional de Defensa Civil (2011) Informe de peligro N° 003-12/05/2011/COEN-SINADECI/15:00 horas (Informe N° 01): Peligro por aluvión en el departamento de Ancash, Huaraz-Peru: COEN-SINADECI, INDECI, Huaraz

Iribarren Anacona P, Mackintosh A, Norton KP (2014) Hazardous processes and events from glacier and permafrost areas: lessons from the Chilean and Argentinean Andes. Earth Surf Process Landf. doi:10.1002/esp.3524

Klimeš J, Vilímek V, Vlčko J (2007) Debris flows in the vicinity of the Machu Picchu village, Peru. In: Sassa K, Fukuoka H, Wang F, Wang G (eds) Progress in landslide science. Springer, pp 313–314

Klimeš J (2012) Geomorphology and natural hazards of the selected glacial valleys, Cordillera Blanca, Peru. AUC Geograph 47:25–31

Klimeš J, Benešová M, Vilímek V, Bouška P, Rapre AC (2014) The reconstruction of a glacial lake outburst flood using HEC-RAS and its significance for future hazard assessments: an example from Lake 513 in the Cordillera Blanca, Peru. Nat Haz 71:1617–1638

Lliboutry L, Morales BA, Pautre A, Schneider B (1977) Glaciological problems set by the control of dangerous lakes in Cordillera Blanca, Peru. I. Historical failures of morainic dams, their causes and prevention. J Glaciol 18:239–254

Morgenstern NR, Price VE (1965) The analysis of the stability of general slip surfaces. Géotechnique 15:70–93

Ng AH-M, Ge L, Li X, Abidin HZ, Andreas H, Zhang K (2012) Mapping land subsidence in Jakarta, Indonesia using persistent scatterer interferometry (PSI) technique with ALOS PALSAR. Int J Applied Earth Obser and Geoinform

Notti D, García-Davalillo JC, Herrera G, Cooksley G (2010) Assessment of the performance of X-band satellite radar data for landslide mapping and monitoring: Upper Tena Valley case study. Nat Hazards Earth Syst Sci 10:1865–1875

Novotný J, Klimeš J (2014) Grain size distribution of soils within the Cordillera Blanca, Peru: an indicator of basic mechanical properties for slope stability evaluation. J Mt Sci 11:563–577

Ojeda N (1974) Consolidacion laguna Palcacocha (in Spanish). Electroperu, Huarás

Oppenheim V (1946) Sobre las lagunas de Huaraz (in Spanish). Boletin Sociedad Geologica Peru., pp 68–80

Oppikofer T, Jaboyedoff M, Keusen H-R (2008) Collapse at the eastern Eiger flank in the Swiss Alps. Nature Geoscience 1:531–535. doi:10.1038/ngeo258

Panizzo A, De Girolamo P, Petaccia A (2005) Forecasting impulse waves generated by subaerial landslides J Geophys Res Ocean 110:23. doi:10.1029/2004jc002778

Portocarrero CAR (2014) The glacial lake handbook—reducing risk from dangerous glacial lakes in the Cordillera Blanca, Peru. USAID technical report, p 80

Rabatel A, Francou B, Soruco A, Gomez J, C'aceres B, Ceballos JL, Basantes R, Vuille M, Sicart JE, Huggel C, Scheel M, Lejeune Y, Arnaud Y, Collet M, Condom T, Consoli G, Favier V, Jomelli V, Galarraga R, Ginot P, Maisincho L, Mendoza J, Menegoz M, Ramirez E, Ribstein P, Suarez W, Villacis M, Wagnon P (2013) Current state of glaciers in the tropical Andes: a multi-century perspective on glacier evolution and climate change. The Cryosphere 7:81–102

Reynolds JM (2011) An introduction to applied and environmental geophysics. Wiley Ltd., p 712

Reynolds JM (2003) Development of glacial hazard and risk minimisation protocols in rural environments. Methods of glacial hazard assessment and management in the Cordillera Blanca Peru. Reynolds Geo-Sciences Ltd., Flintshire, p 72

Richardson SD, Reynolds JM (2000) Degradation of ice-cored moraine dams: implications for hazard development. IAHS Publications 264:187–197

Righini G, Pancioli V, Casagli N (2011) Updating landslide inventory maps using Persistent Scatterer Interferometry (PSI). Int J Remote Sens 33:1–29

Rosen P, Hensely S, Joughin I, Li F, Madsen S, Rodriguez E (2000) Goldstein R (2000) Synthetic aperture radar interferometry. Proc IEEE 88:333–382

Schneider-Muntau B, Zangerl C (2005) Numerical modelling of a slowly creeping landslide in crystalline rock—a case study. In: Konečný P (ed) Impact of human activity on the geological environment. Taylor & Francis Group plc, London, pp 535–540

Schneider D, Huggel C, Cochachin A, Guillén S, García J (2014) Mapping hazards from glacier lake outburst floods based on modelling of process cascades at Lake 513, Carhuaz, Peru. Adv Geosci 35:145–155

Simeoni L, Tarantino A, Mongiovi L (2003) Effects of unsaturation on the stability of a moraine slope. In: Schanz T (ed) Unsaturated soils: experimental studies, Proceedings of the International Conference, From Experimental Evidence towards Numerical Modeling of Unsaturated Soils, Weimar, Germany., pp 497–508

Somos-Valenzuela M, Chisolm RE, McKinney DC, Rivas D (2014) Hazard mapping of a potential glacial lake outburst flood in Huaraz, Peru. Center for research in water resources, Online Report 14–01. http://www.crwr.utexas.edu/online.shtml. Accessed 21 November 2014

Springman SM, Jommi C, Teysseire P (2003) Instabilities on moraine slopes induced by loss of suction: a case history. Géotechnique 53:3–10

Strozzi T, Wegmüller U, Tosi L, Bitelli G, Spreckels V (2001) Land subsidence monitoring with differential SAR interferometry. Photogramm Eng Remote Sens 67:1261–1270

Strozzi T, Farina P, Corsini A, Ambrosi C, Thuring M, Zilger J, Wiesmann A, Wegmüller U, Werner C (2005) Survey and monitoring of landslide displacements by means of L-band satellite SAR interferometry. Landslides 2:193–201

Strozzi T, Ambrosi C, Raetzo H (2013) Interpretation of aerial photographs and satellite SAR interferometry for the inventory of landslides. Remote Sens 5:2554–2570. doi:10.3390/rs5052554

Sun Q, Zhang L, Ding Y, Hu J, Liang H (2015) Investigation of slow-moving landslides from ALOS/PALSAR images with TCPInSAR: a case study of Oso, USA. Remote Sensing 7:72–88

Tamburini A, Del Conte S, Larini G, Lopardo L, Malaguti C, Vescovi P (2011) Application of SqueeSARTM to the characterization of deep seated gravitational slope deformations: the Berceto case study (Parma, Italy). In: Margottini C, Canuti P, Sassa K (eds) Landslide science and practice, vol 2. Springer, New York, pp 437–444, Early Warning, Instrumentation and Monitoring

Viero A, Teza G, Massironi M, Jaboyedoff M, Galgaro A (2010) Laser scanning-based recognition of rotational movements on a deep seated gravitational

instability: the Cinque Torri case (North-Eastern Italian Alps). Geomorphology 122:191–204. doi:10.1016/j.geomorph.2010.06.014
Vilímek V, Zapata ML, Klimeš J, Patzelt Z, Santillán N (2005) Influence of glacial retreat on natural hazards of the Palcacocha Lake area, Peru. Landslides 2:107–115
Vilímek V, Klimeš J, Červená L (2015) Glacier-related landforms and glacial lakes in Huascarán National Park, Peru. J Maps doi. doi:10.1080/17445647.2014.1000985
Wegmüller U, Werner C, Strozzi T, Wiesmann A (2003) Multi-temporal interferometric point target analysis. In: Proceedings of the Multi-Temp Conference, Ispra, Italy, 16–18 July 2003
Werner C, Wegmüller U, Strozzi T, Wiesmann A (2003) Interferometric point target analysis for deformation mapping. In Proceedings of IGARSS, Toulouse, France, 21–25 July 2003
Westoby MJ, Glasser NF, Brasington J, Hambrey MJ, Quincey DJ, Reynolds JM (2014) Modelling outburst floods from moraine-dammed glacial lakes. Earth-Sci Rev 134:137–159
Worni R, Huggel C, Clague JJ, Schaub Y, Stoffel M (2014) Coupling glacial lake impact, dam breach, and flood processes: a modeling perspective. Geomorphology 224:161–176
Yamada T (1998) Glacier lake and its outburst flood in the Nepal Himalaya., Japanese Society of Ice and Snow
Zapata ML (2002) La dinamica glaciar en lagunas de la Cordillera Blanca (in Spanish). Acta Montana 19:37–60